



HAL
open science

Thermodynamic analysis of a 200 MWh electricity storage system based on high temperature thermal energy storage

Kévin Attonaty, P Stouffs, Jérôme Pouvreau, Jean Oriol, Alexandre Deydier

► **To cite this version:**

Kévin Attonaty, P Stouffs, Jérôme Pouvreau, Jean Oriol, Alexandre Deydier. Thermodynamic analysis of a 200 MWh electricity storage system based on high temperature thermal energy storage. *Energy*, 2019, 172, pp.1132-1143. 10.1016/j.energy.2019.01.153 . hal-02153245

HAL Id: hal-02153245

<https://univ-pau.hal.science/hal-02153245>

Submitted on 22 Oct 2021

HAL is a multi-disciplinary open access archive for the deposit and dissemination of scientific research documents, whether they are published or not. The documents may come from teaching and research institutions in France or abroad, or from public or private research centers.

L'archive ouverte pluridisciplinaire **HAL**, est destinée au dépôt et à la diffusion de documents scientifiques de niveau recherche, publiés ou non, émanant des établissements d'enseignement et de recherche français ou étrangers, des laboratoires publics ou privés.



Distributed under a Creative Commons Attribution - NonCommercial 4.0 International License

Thermodynamic analysis of a 200 MWh electricity storage system based on high temperature thermal energy storage

Kevin Attonaty ^{a,b}, Pascal Stouffs ^b, Jérôme Pouvreau ^c, Jean Oriol ^a,
Alexandre Deydier ^d

^a CEA, CTREG, DNAQU, F-33600 Pessac, France

^b Univ. Pau & Pays Adour/E2S UPPA, Laboratoire de Thermique, Energétique et Procédés - IPRA, EA1932, F-64000 Pau, France

^c Univ. Grenoble Alpes, CEA, LITEN, DTBH, LST, F-38000 Grenoble

^d Babcock Wanson, F-47600 Nérac, France

Abstract

With the increase in the share of intermittent renewable energies as part of the global energy mix comes the issue of energy storage. This work concerns a power-to-power electricity storage relying on sensible storage at high temperature (900 °C). A focus is put on finding the best compromise between the valorization of the stored energy and the optimal functioning of the power-to-power process. The charging loop is made of an electrical heater and fans, while the conversion of the stored heat to electricity can be done in a gas cycle or a combined cycle. To set up a relevant base design for the system, the reciprocal influence of the storage and the discharging cycle needs to be evaluated. A thermodynamic modeling was therefore carried on and first and second law (or exergy) analyses were performed. Results show that the choice of the discharging cycle has a high impact on the sizing of the storage, by inducing different levels of pressure or temperature. Adding combustion in the discharging phase allows to achieve a better power-to-power efficiency and to reduce the storage volume, but also involves a fuel consumption that is not negligible. Finally, the power-to-heat conversion leads to high exergy destructions in the charging loop but thanks to the high temperature of the storage, this exergy destruction is not excessive when compared to conventional heat input from combustion systems.

Highlights

- The round-trip efficiency reaches around 50% in a combined cycle with combustion.
- The electricity to heat conversion at 900 °C destroys about 30 % of the inlet exergy.
- Three possible architectures of the system have been studied.
- Energy release in a gas cycle was found to be poorly efficient.
- Packed bed thermal storage represents less than 10 % of the global exergy destruction.

Keywords: *exergy analysis, combined cycle power plant, thermal energy storage, packed bed, thermodynamics*

Nomenclature	
A	Viscous parameter of the Ergun equation
a_{sol}	Surface area of solid per unit bed volume ($m^2 \cdot m^{-3}$)
a_w	Surface area of packed bed per unit bed volume ($m^2 \cdot m^{-3}$)
b	Parameter of the gas turbine cooling model, or Specific exergy, ($J \cdot kg^{-1}$)
B	Inertial parameter of the Ergun equation, or Exergy, (J)

\dot{B}_D	Exergy destruction rate, (W or J.s ⁻¹)
c_p	Specific heat capacity, (J.kg ⁻¹ .K ⁻¹)
D	Diameter, (m)
e_f	Specific internal energy of the fluid, (J.kg ⁻¹)
E	Energy, (J)
E_e	Electrical energy, (J)
h	Specific enthalpy, (J.kg ⁻¹)
H	Enthalpy, (J)
H_b	Height of the packed bed, (m)
k	Parameter of the effective heat transfer coefficient calculation
LHV	Lower heating value, (J.kg ⁻¹)
m	Mass, (kg)
\dot{m}	Mass flow rate, (kg.s ⁻¹)
\dot{m}_{cool}	Gas turbine cooling mass flow rate, (kg.s ⁻¹)
P	Pressure, (Pa)
PR	Pressure ratio, (-)
Q	Heat, (J)
s	Specific entropy, (J.kg ⁻¹ .K ⁻¹)
\dot{S}_{gen}	Entropy generation rate, (W.K ⁻¹)
t	Time, (s)
t_{ins}	Insulation thickness, (m)
T	Temperature, (°C)
$T_{b,lim}$	Gas turbine limit blade temperature, (°C)
u	Fluid velocity, (m.s ⁻¹)
U	Overall heat transfer coefficient of the tank walls, (W.m ⁻² .K ⁻¹)
V	Volume, (m ³)
W	Work, (J)
ΔT_{ap}	Approach temperature difference at the superheater, (°C)
ΔT_{pp}	Pinch point temperature difference at the evaporator, (°C)
Greek symbols	
α	Heat transfer coefficient, (W.m ⁻² .K ⁻¹)
ε	Packed bed void fraction, (-)
λ	Thermal conductivity, (W.m ⁻¹ .K ⁻¹)
η	Efficiency, (-)
ρ	Density, (kg.m ⁻³)
τ	Utilization rate of the storage tanks, (-)

μ	Dynamic viscosity, (Pa.s)
Abbreviations	
CCGT	Combined Cycle Gas Turbine
GC	Gas cycle
GT	Gas turbine
HTF	Heat transfer fluid
SC	Steam cycle
ST	Steam turbine
Subscripts	
0	At ambient conditions (15 °C, 1 atm)
b	packed bed
c	kinetic
Ca	Carnot
cond	condenser
comb	combustion
comp	compressor
eff	effective
elec	electrical
exh	exhaust gases
exp	expansion device
ext	external
f	fluid
heater	electrical heater
ins	insulation
is	isentropic
l	liquid
max	Maximum
mech	Mechanical
p	Potential
P2P	Power-to-power
sat	Saturation
sol	Solid
st	Steam
stor	Storage
th	Thermal

1. Introduction

In a context of global warming and increasing scarcity of natural resources, renewable energies tend to get more and more attraction. Following a recent report from the Renewable Energy Policy Network for the 21st Century (REN 21), renewables now represent more than 50 % of the yearly net additions to the global power generating capacity [1]. Solar photovoltaics and wind farms represent most of these new capacities. With decreasing costs and geographical flexibility, these solutions are expected to allow a more sustainable energy mix. On the other hand, the aforementioned renewable resources come with unavoidable intermittence, causing potential issues between the electricity injected to the power grid and the consumers' needs. Efficient energy storage solutions could allow to store the energy when there is no need for it and release it when the production cannot sustain the demand.

Several energy storage solutions coexist and involve different characteristics of capacity, power, cost and technological maturity. A focus on the available technologies for large scale applications brings out pumped hydroelectric storage (PHS), compressed air energy storage (CAES) and batteries [2]. Another way to store massive amounts of energy – at least a few hundred megawatt-hours - is thermal energy storage (TES). It is often laid aside because of its close relationship with Concentrated Solar Power (CSP) plants, which makes it look like a solution dedicated to the storage of solar heat. However, several studies showed its interest for power-to-power applications, from pumped thermal electricity storage (PTES) to its integration in CAES systems to form adiabatic CAES (A-CAES) processes [3]–[7].

Heat storage technologies are generally arranged in three categories with decreasing technological maturities: sensible thermal energy storage, latent thermal energy storage and chemical heat storage [8]. The state-of-the-art large scale TES technology is the two-tanks molten salt storage [9]. In this type of system, the fluid circulates between a cold tank and a hot tank. The charging phase often involves solar heat and the discharging phase a steam (or Rankine) thermodynamic cycle. This type of system has been applied at a very large scale (1010 MWh_{th} in Andasol CSP power plant in Spain [10]). Despite its technological maturity, it suffers from several drawbacks: the molten salts have high and low temperature limits, their long-term availability is uncertain and their toxicity can cause environmental damage in case of a fluid leakage.

In order to reduce the cost of this type of storage, the single-tank packed-bed storage has emerged. In this concept, some of the storage fluid is replaced by a solid material, and only one tank is needed. To benefit from thermal stratification and preserve the quality of the stored energy, the hot fluid enters by the top of the tank during charge and the cold fluid enters by the bottom during discharge. This leads to the creation of a thermal gradient zone which is known as the “thermocline” (Figure 1) [9]. The state-of-the-art single-tank configuration is the one that has been applied in the USA for the Solar One project (182 MWh_{th}), with rocks and sand as filler material and thermal oil as heat transfer fluid (HTF) [10]. Despite its advantages, this technology shares some of the drawbacks of the two tanks system, namely the environmental impact of the fluid and its cost, and the need to insure a good and lasting compatibility between the HTF and the solid filler material [11]. Moreover, oversizing can be required because of the volume filled by the thermal gradient.

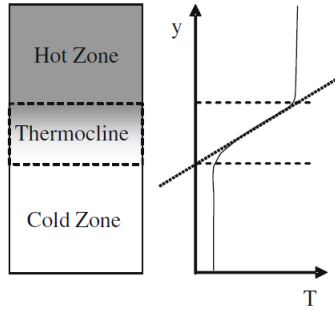


Figure 1. Schematic representation of the thermocline zone in a single tank thermal energy storage [12].

An emerging proposal is to replace the liquid HTF with air. When compared to conventional HTFs, air is free, non-toxic and non-inflammable. Moreover, it has no upper or lower temperature limit, meaning that the storage can be operated with a higher temperature difference, offering the possibility to raise the energy density. The energy stored in an air/packed bed storage tank is equal to the energy stored in the solids, due to air weak thermal properties. The expression of this sensible heat is given in Equation (1).

$$Q_{stor} = \int_{T_{charge}}^{T_{discharge}} m_{sol} c_{psol} dT \quad (1)$$

Furthermore, the higher outlet temperature during discharge can lead to a better thermal efficiency of the heat to electricity conversion process. This is pointed out by the Carnot efficiency, which is the maximal theoretical efficiency of a thermal system (Equation (2)).

$$\eta_{Ca} = 1 - \frac{T_{cold}}{T_{hot}} \quad (2)$$

Packed bed storages with air as HTF tend to get more and more attention in the recent literature [13]–[16]. However, to the authors' knowledge, they do not show a lot of commercial realizations, at the exception of Airlight Energy's Ait Baha CSP pilot plant, which includes an air/bedrock storage with a conical shape for mechanical stability and an upper temperature of about 600 °C [17]. For technical and economic reasons, the storage upper temperature was set in this study to 900 °C to insure insulation and storage material availability [18].

2. EMR'Stock system description

The proposed system is shown in Figure 2. Its outline architecture is based on the generic architecture of a combined cycle power plant, providing a majority of state-of-the-art components with an interesting level of technological maturity. The heat storage at 900 °C is done in several tanks filled with solid spheres. In the discharging phase (framed in red in Figure 2), the storage brings heat to the cycle. The opportunity to add combustion to increase the thermal efficiency will be evaluated. In the charging phase, the combined cycle is stopped and a set of valves and pipes allows to charge the storage with an independent

charging loop (framed in blue) which will be described thereafter. In Figure 2, the number of storage tanks is only indicative.

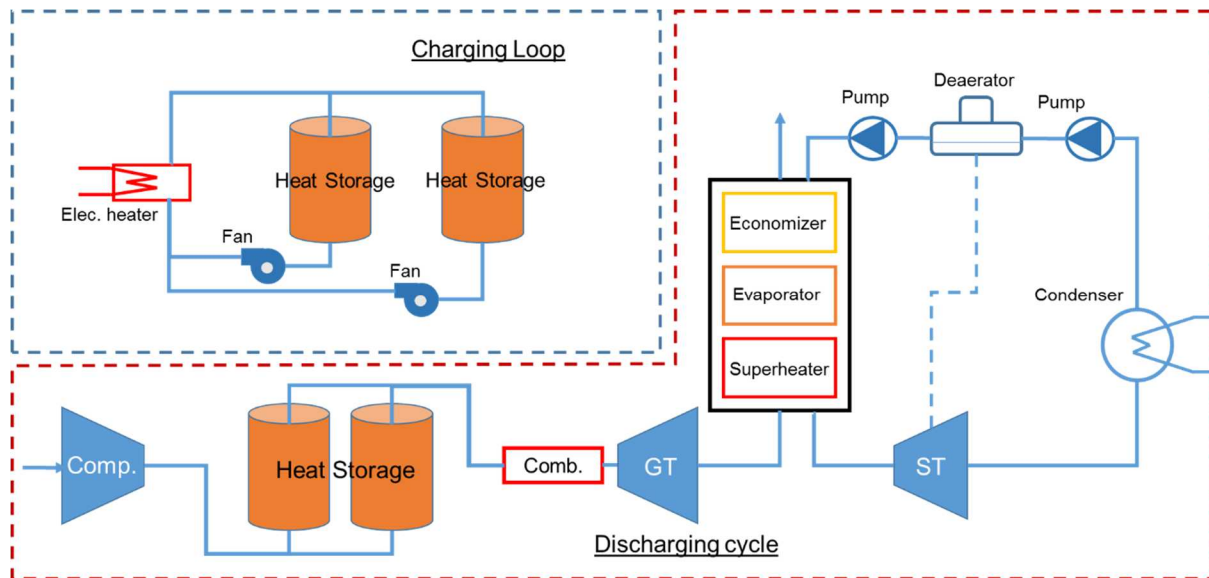


Figure 2. Schematic representation of the power-to-power storage system (the connections between the charging loop and the cycle are not shown).

2.1. Description of the power-to-power process

The charging loop includes an electric heater which converts electricity into heat, precisely by heating air up to 900 °C. The heat exchange between the hot air and the solid filler material charges the tanks. The time length of this phase is five hours, which is a typical schedule of electricity production from a wind farm, during night time. The fans outlet temperature cannot be superior to 800 °C after these five hours, a technical limit which seems to be unavoidable and prevents from operating full charges of the tanks [19].

Following a representative standby of three hours, the system releases the stored energy by the means of a combined cycle. This discharge lasts three hours, which is typically the duration of a peak of consumption on the power grid. Its functioning follows the standard process of CCGT power plants, with the heat released from the storage as a heat source of the gas cycle. Ambient air enters the gas compressor and is pressurized in the process. The resulting air flows through the storage tanks and recovers heat from them. Air can be further heated with additional combustion and is finally expanded in the gas turbine (GT) before exiting the gas cycle (also called Joule or Brayton cycle). The thermal stratification of the storage insures a constant outlet temperature during most of the discharge. This temperature starts to decrease when the thermal gradient leaves the tanks. In the base case (without combustion), the mass flow rate of the gas cycle is set to get a temperature of 850 °C at the inlet of the GT after three hours of discharge, to remain close to the GT design point. In the case of additional combustion, the flow rate is set to get a temperature difference of 50 °C between the inlet and outlet of the storage after three hours, leading to almost full discharges of the tanks. The particularity of a combined cycle power plant is that a steam cycle (also called Rankine cycle) is designed to recover the remaining heat of the gas turbine exhaust gases. To this extent, water is pumped into a component called Heat Recovery Steam Generator (HRSG), composed of three sections of heat exchangers: economizer, evaporator

and superheater. Steam is then expanded in the steam turbine (ST), before reaching liquid state in the condenser to close the Rankine cycle [20].

2.2. Design considerations for the thermal energy storage

Several storage materials are available to store heat at the considered level of temperature [18]. This study will rely on the use of alumina spheres, because their ability to withstand cycling at very high temperatures has already been proved and their industrial supply is supposed to be reliable [15], [21], [22]. The thermal properties of this material were modeled following the experimental characterizations from Munro [22] (Table 1).

Table 1. Modeling of the thermal properties of 99.5 % pure alumina spheres (20-1800 °C)

Thermal property	Model [21]
ρ_{sol} (kg.m ⁻³)	3931
$c_{p,sol}$ (J.kg ⁻¹ .K ⁻¹)	$1117 + 0.14 T(^{\circ}\text{C}) - 411 \exp(-0.006 T(^{\circ}\text{C}))$
λ_{sol} (W.m ⁻¹ .K ⁻¹)	$5,85 + 15360 \exp(-0,002 T(^{\circ}\text{C})) / (T(^{\circ}\text{C}) + 516)$

To size the storage tanks, a height to diameter ratio of 1 was considered. Several authors showed that increasing this ratio to look for a better thermal efficiency leads to counter-productive effects because of the increasing pressure drop and thermal losses [23]. The proposed value leads to a tradeoff between these constraints.

As shown in Figure 2, the pressurized air flowing out of the gas compressor enters in the thermal storage during the discharge. The consequence is that the maximal pressure of the gas cycle is also the maximal pressure in the storage tanks. Communication with an industrial partner gave the maximal dimensions of the tanks to insure their industrial feasibility with a common material (310S stainless steel). These dimensions are given in Table 2 for an aspect ratio H_b/D_b equal to 1, and for two different levels of pressure.

Table 2. Maximal dimensions for the sensible thermal energy storage.

Maximal pressure	Maximal tank dimensions	Maximal bed dimensions ($t_{ins} = 0.4$ m)
10 bar	$H_{tank,max} = 11$ m	$H_{b,max} = 10,2$ m
	$L_{tank,max} = 11$ m	$L_{b,max} = 10,2$ m
15 bar	$H_{tank,max} = 5,55$ m	$H_{b,max} = 4,75$ m
	$L_{tank,max} = 5,55$ m	$L_{b,max} = 4,75$ m

The storage tanks need internal insulation to insure an appropriate wall temperature. The insulation thickness t_{ins} (0.4 m in this study) has to be considered to deduce the maximal packed bed volume in each tank. For instance, it only leaves 4.75 m x 4.75 m of useful storage volume in one tank if the maximal pressure is set to 15 bar (see Table 2).

This study will consider the effects of the hybridization between the storage tanks and the cycle to evaluate the potential of such a system. In order to optimize such a system in future studies, there is a need for knowledge on its functioning and on its energy and exergy efficiency. To answer these questions, a thermal model was set.

3. Thermodynamic model of the system

The model was developed using the software Dymola, with the object-oriented language Modelica. The Radau solver with a tolerance of $1e^{-6}$ was selected to solve the equations. Several usual assumptions for modeling of thermodynamic cycles at a system scale were made:

- Ideal gas assumption (with temperature-dependent specific heat, thermal conductivity and dynamic viscosity).
- Adiabatic compression/expansion processes with constant isentropic efficiencies.
- No thermal losses for the heat exchangers.
- Steady state is assumed (at the exception of the thermal storage).

The transient behavior of the storage is considered because it is expected that it will influence the behavior of the downstream system. In terms of dynamics, the time length of the cycles – from three hours for the discharge to five hours for the charge – is long enough to neglect the start-ups and shutdowns of turbomachinery.

3.1. Components thermodynamic models

The model is based on the first law of thermodynamics, i.e. energy conservation (Equation (3)). In this work, kinetic and potential energy $\Delta\dot{E}_c$ and $\Delta\dot{E}_p$ will be neglected.

$$\dot{W} + \dot{Q} = \Delta\dot{H} + \Delta\dot{E}_c + \Delta\dot{E}_p \quad (3)$$

3.1.1. Compression work

All the compression devices (compressor, fans, and pumps) are modeled following the same approach. Instantaneous work is computed with Equation (4).

$$\dot{W} = \dot{m}(h_{out} - h_{in}) \quad (4)$$

The specific outlet enthalpy h_{out} is determined by setting an isentropic efficiency for the transformation. The real outlet enthalpy is deduced from the outlet enthalpy of a fictive ideal transformation (Equation (5)).

$$\eta_{is,comp} = \frac{h_{out,is} - h_{in}}{h_{out} - h_{in}} \quad (5)$$

$$s(P_{in}, T_{in}) = s(P_{out}, T_{out,is}) \quad (6)$$

In this study, the pressure ratio (PR) of a gas cycle is defined as the ratio between the outlet and inlet pressure of the compressor.

3.1.2. Expansion work

Following the methodology described for the compression processes, expansion work (i.e. gas turbine, steam turbine) is defined with its isentropic efficiency (Equation (7)).

$$\eta_{is,exp} = \frac{h_{in} - h_{out}}{h_{in} - h_{out,is}} \quad (7)$$

The output power of the turbine is then computed with Equation (4). At high temperatures, the gas turbine needs a cooling flow rate which is extracted from the compressor outlet. It is evaluated with the approach from [24].

$$\dot{m}_{cool} = \dot{m}_{GT} b (c_{p,air,comp} / c_{p,exh,GT}) ((T_{GT,in} - T_{b,lim}) / (T_{b,lim} - T_{comp,out})) \quad (8)$$

In this expression, the parameter b has a value of 0.154 and the limit turbine blade temperature $T_{b,lim}$ has a value of 880 °C. This cooling flow rate is neglected for the cases without combustion ($T_{GT,in} \leq 900$ °C $\approx T_{b,lim}$).

3.1.3. Combustion

The combustor model assumes complete combustion of pure methane (CH_4). The thermal losses through the walls of the combustion chamber are neglected. The energy balance for the combustion transformation is:

$$\dot{m}_{air}h_{air,in} + \dot{m}_{CH_4}LHV_{CH_4} + \dot{m}_{CH_4}h_{CH_4,in} = (\dot{m}_{air} + \dot{m}_{CH_4})h_{exh} \quad (9)$$

In which the specific enthalpy of exhaust gases h_g and inlet mass flow rate of fuel \dot{m}_{CH_4} are computed from the chemical reaction of combustion of CH_4 with air and the desired adiabatic combustion temperature, which is a parameter of the model. Composition of outlet gases is also computed from this reaction of combustion. The pressure drop across the combustion chamber is considered as 5 % of the incoming air pressure, a common value from the literature (see for example [25], [26]).

3.1.4. Heat exchangers

The model for the heat exchangers from the HRSG is the standard heat energy balance equation described in Equation (10).

$$\dot{m}_{water}(h_{out,water} - h_{in,water}) + \dot{m}_g(h_{out,exh} - h_{in,exh}) = 0 \quad (10)$$

Several design parameters were added to take into account some technological constraints: the approach temperature difference ΔT_{ap} at the superheater, the pinch point temperature difference at the evaporator ΔT_{pp} and the maximal steam temperature $T_{max,st}$. The values of these parameters, and the other ones involved in the model, are introduced in Table 3.

3.1.5. Condenser

The condenser is not modeled as a conventional heat exchanger but as a heat sink able to condensate the inlet steam, regardless of its inlet conditions. With this approach, the amount of heat leaving the condenser is computed as follow:

$$\dot{Q}_{cond} = \dot{m}_{water}(h_{l,sat}(P_{in}) - h_{in}) \quad (11)$$

3.1.6. Deaerator

The deaerator makes sure that the inlet water of the HRSG does not contain any dissolved gases. At the outlet of the condenser, the water flows through a first pump and is then brought to saturation to expel the gases. It is done by injection of steam from the steam turbine. The dissolved gases outlet flow rate being negligible when compared to the other streams, the energy conservation in steady state is:

$$\dot{m}_{in,water}h_{in,water} + \dot{m}_{in,steam}h_{in,steam} = \dot{m}_{out,water}h_{out,water} \quad (12)$$

A deaerator operating pressure of 1.2 bars is assumed, and the steam is extracted at 5 bars from the steam turbine. These typical values were taken from a manufacturers' documentation [27].

Table 3. Main parameters of the thermal model

Parameter	Value
$\eta_{is,comp}$	0.88
$\eta_{is,GT}$	0.89
$\eta_{is,ST}$	0.85
$\eta_{is,pumps}$	0.85
η_{fans}	0.85
η_{heater}	0.98
η_{mech}	0.98
η_{elec}	0.98
$T_{max,st}$	560 °C
ΔT_{ap}	20 °C
ΔT_{pp}	10 °C
ΔP_{comb}	5 %
ΔP_{heater}	0.15 bar

3.1.7. Electric heat source

The electric heater involved in the charging loop is a heat source enable to heat air up to 900 °C, regardless of its inlet state. This is consistent with the behavior of such an electric heater, which offers a flexible power.

$$\dot{Q}_{heater} = \dot{m}_{air}(h_{out}(T_{max,air}, P_{in} - \Delta P_{heater}) - h_{in}(T_{in}, P_{in})) \quad (13)$$

An electricity-to-heat efficiency is also defined for this component to consider some electrical losses. This efficiency has a value of 0.98 (Equation (14)).

$$\dot{Q}_{heater} = \eta_{heater} \dot{E}_{e,heater} \quad (14)$$

3.1.8. Sensible thermal energy storage

The thermal model of the packed-bed TES follows the classical approach of the two equations model originally proposed by Schumann in 1929 [28]. This model was enhanced by several authors to expand its exhaustiveness. In this work, the formulation of [9] (also used in [29]) was considered. It is a generic model which offers to consider the axial thermal conduction in the solid and the fluid phase as well as thermal losses to the outside of the tank. This model is computed with two energy balances (one for the fluid and one for the solid filler material) given in Equations (15) and (16).

$$\varepsilon \left(\frac{\partial(\rho_f e_f)}{\partial t} + \frac{\partial(u \rho_f h_f)}{\partial z} \right) = \frac{\partial}{\partial z} \left(\lambda_{eff,f} \frac{\partial T_f}{\partial z} \right) + \alpha_{eff} a_{sol} (T_{sol} - T_f) + U_w a_w (T_0 - T_f) \quad (15)$$

$$(1 - \varepsilon) \rho_{sol} c_{p,sol} \frac{\partial T_{sol}}{\partial t} = \frac{\partial}{\partial z} \left(\lambda_{eff,sol} \frac{\partial T_{sol}}{\partial z} \right) + \alpha_{eff} a_{sol} (T_f - T_{sol}) \quad (16)$$

The thermal losses to the ambient air are included in the last term of the fluid energy balance (15) because the solid contact area with the tank walls is considered negligible when compared to the contact area between the fluid and the walls. This model also involves the following assumptions [9]:

- Homogeneous porous medium in all directions.
- Mono-dimensional heat transfer.
- Plug flow velocity profile for the fluid.

A mono-dimensional spatial discretization is set in the Dymola model to solve equations (15) and (16). To extend the validity of the Schumann type model to cases in which the solids conduction resistance is not negligible, Stuke proposed to introduce an effective heat transfer coefficient [30] (Equation (17)). Xu & al. showed that this approach leads to very satisfying results when compared to more complex analytical resolution of conduction in the solids, and is valid for Biot numbers up to 100 [31]. k is a constant which is equal to 10 for spheres.

$$\frac{1}{\alpha_{eff}} = \frac{1}{\alpha} + \frac{D_{sol}}{\lambda_{sol}k} \quad (17)$$

α is computed with the classic correlation from Wakao & al which gives satisfying results for packed beds made of uniform spheres [32]. $\lambda_{eff,f}$ and $\lambda_{eff,sol}$ are evaluated with the method from [9] using Zehner & Schlunder's model [33] with Breitbach addition for the contribution of radiation between solids to the thermal diffusion [34] and Wakao & al formulation for the contribution of the fluid mixing [35]. Pressure drop in the packed bed is computed following the classical Ergun formulation from Equation (18) [36].

$$\frac{\Delta P}{L} = A \frac{(1-\varepsilon)^2 \mu_f(\varepsilon u)}{\varepsilon^3 D_{sol}^2} + B \frac{(1-\varepsilon) \rho_f(\varepsilon u)^2}{\varepsilon^3 D_{sol}} \quad (18)$$

A and B are experimental coefficients which have been discussed in the literature. As it was not possible to perform experimental measurements of pressure drop in the present case, the original Ergun values, respectively 150 and 1.75, were used to evaluate the pressure drop at this low stage of project definition. The overall heat transfer coefficient with the outside U_w is computed by considering that the convective resistances in and out of the tank are negligible when compared to the conduction resistance of the insulation material. The main parameters of the storage model are compiled in Table 4.

Table 4. Main parameters of the thermal energy storage model

Parameter	Value
D_{sol}	0.03 m
ε	0.37
λ_{ins}	0.15 W.m ⁻¹ .K ⁻¹
t_{ins}	0.4 m
H_b/D_b	1

3.2. Energy analysis

The model described above was used to evaluate the thermodynamic performance of the system. The combined cycle thermal efficiency is computed with Equation (19), and real electric efficiency is deduced from it by applying two corrections factors accounting for mechanical efficiency and electric generator efficiency, both equal to 0.98 (Equation (20)).

$$\eta_{th,CCGT} = \frac{(|\dot{W}_{GT}| - |\dot{W}_{comp}|) + (|\dot{W}_{ST}| - |\dot{W}_{pump}|)}{\dot{m}_{air}(h_{out,stor} - h_{in,stor}) + \dot{m}_{exh}(h_{out,comb} - h_{in,comb})} \quad (19)$$

$$\eta_{CCGT} = \eta_{th,CCGT} \eta_{mech} \eta_{elec} \quad (20)$$

A global power to power (or round-trip) efficiency is also defined following Equation (21):

$$\eta_{P2P} = \frac{E_{e,out}}{E_{e,in}} \quad (21)$$

With the inlet and outlet energy given by:

$$E_{e,in} = \int_0^{t_{charge}} (\dot{E}_{e,heater} + \dot{E}_{e,fans}) dt \quad (22)$$

and:

$$E_{e,out} = \int_0^{t_{discharge}} \dot{E}_{e,CCGT} dt \quad (23)$$

When it is plugged in a thermal system, the thermal storage does not achieve complete charge-discharge cycles. It means that the tanks need to be oversized. The utilization rate is used to compare the stored energy to the maximal energy that could be stored, if the thermocline zone was completely released in each charge and discharge:

$$\tau_{stor} = \frac{Q_{stor,charge}}{Q_{max,stor}} \quad (24)$$

In this relation, $Q_{max,stor}$ is the maximal storable energy defined in Equation (1).

3.3. Exergy analysis

Exergy analysis is based upon the second principle of thermodynamics. It introduces an energy quality criterion, which does not appear in the energy conservation from the first principle, in which every equal amount of energy has the same value. For example, the exergy analysis will assign more value to a heat source at high temperature than to a heat source at low temperature, because its ability to produce work is higher. This approach also gives the possibility to quantify the degree of perfection of thermodynamic systems by the means of exergy destruction (also called irreversibilities or availability losses) calculation and analysis. Exergy is defined with Equation (25), the 0 subscripts referring to a reference state, defined here as ambient conditions of (15 °C, 1 atm).

$$B = (H - H_0) - T_0(S - S_0) \quad (25)$$

Following a definition from Bejan & al. [37], the expression of the transient exergy balance for an open fluid control volume is:

$$\frac{dB}{dt} = \sum \left(1 - \frac{T_0}{T_j} \right) \dot{Q}_j - \left(-\dot{W} - P_0 \frac{dV}{dt} \right) + \dot{m}_{in} b_{in} - \dot{m}_{out} b_{out} - \dot{B}_D \quad (26)$$

The value of the exergy destruction from each component \dot{B}_D is deduced from this expression. For all the components except the thermal storage, steady state is assumed, which simplifies the above expression by equaling the left term to zero. Concerning the thermal energy storage, the exergy destruction balance is introduced in Equation (27) for a control volume made of solids and a fluid considered as an ideal gas [37]. This balance is deduced from the equivalence between exergy destruction and entropy generation. The thermal processes in the storage (convection, conduction...) are internal to the control volume.

$$\dot{B}_{D,storage} = T_0 \dot{S}_{gen,tot} = T_0 \left[\dot{m}(s_{out} - s_{in}) + \frac{dS}{dt} - \frac{\dot{Q}_{losses}}{T_0} \right] \quad (27)$$

The term with a time derivative accounts for entropy variation rate in both the solid phase and the fluid phase of the control volume (Equation (28)). The mass of fluid in the control volume is considered negligible when compared to the mass of solid. Indeed, the density of the solid is about three orders of magnitude higher than the density of the fluid in the considered pressure and temperature conditions, and the volume of fluid is about a third of the control volume.

$$\frac{dS}{dt} = \frac{dS_{sol}}{dt} = m_{sol} c_{psol} \frac{1}{T_{sol}} \frac{dT_{sol}}{dt} \quad (28)$$

4. Description of the studied cases

This study focuses on a 200 MWh_e power-to-power storage system. Three cases were compared. In the first case, the discharge does not involve any combustion. The consequence is that the gas turbine inlet temperature is set by the outlet temperature profile in the storage. In the second case, additional combustion completes the heat supplied by the storage. The role of the combustion is to increase the temperature of the air entering the gas turbine and to allow almost full discharges of the storage. An intermediate level of temperature of 1200 °C is considered for the combustion. Moreover, combined cycles are expensive systems which are usually recommended for high power applications. To check the performances of a cheaper system, a last case of a discharge in a simple gas cycle without combustion was studied.

For each case, the pressure ratio PR of the gas cycle and the pressure level of the steam cycle were set to optimize the thermal efficiency of the combined cycle. The other parameters were set to relevant values from the literature (see previous Tables 3 and 4).

5. Results and discussion

In the following part, the results of the case studies are introduced. For each case, the energy efficiencies of the global power-to-power process and of the discharging cycle are given. A second law analysis of each scenario highlights the share of exergy destruction in the system and the critical components from a thermodynamic point of view.

5.1. Base case: release in a combined cycle without combustion

This system is the one introduced in Figure 2, but does not include any combustion. As a consequence, the gas turbine inlet temperature is around 900 °C at the beginning of the discharge, until it starts to decrease when the thermocline zone starts to leave the tank. For this study, the discharge mass flow rate is set to get a turbine inlet temperature of 850 °C after three hours. This means that the storage tanks are not fully discharged after each energy release phase.

The main thermal model results are shown in Table 5. To limit the pressure drop in the storage at an acceptable value (inferior to 0.15 bar) during charge, the storage volume was divided in two tanks operated in parallel. This table introduces the results from a stabilized cycle, meaning that a few cycles were run before to reach a cyclic state representative of the day-to-day functioning of the storage system.

Table 5. Thermal model results of the base case.

Variable	Value
$V_{stor,tot}$	577 m ³ ($L_b=D_b=7.16\text{m}$, $n_{tanks} = 2$)
\dot{m}_{charge}	74.6 kg.s ⁻¹
$\Delta P_{stor,charge}$	~ 0.11 bar

$\dot{m}_{discharge}$	98.8 kg.s ⁻¹
PR	10
$P_{in,st}$	29 bar
$E_{e,in}$	200 MWhe
η_{CCGT}	0.43
$E_{e,out}$	82 MWhe
η_{P2P}	0.41
τ_{stor}	0.71

The pie chart of Figure 3 shows the energy distribution on a whole charge-discharge process. 28 % of the inlet energy leaves the system with the exhaust gases at the outlet of the heat recovery steam generator. It is a common conclusion of the energy analysis of a combined cycle, because the remaining energy of the expanded gases cannot be entirely recovered to produce steam. The important share of condenser losses (25 % of the inlet energy) is also a classic result showing that a lot of heat is released to close the steam cycle. Because of these two contributions, the major part of the heat losses occurs during discharge.

More interesting aspects are the weak share of thermal losses at the storage component at a cycle scale. The large volume of the tank offers a low external area per unit of volume. Furthermore, the assumption for the thermal insulation implied that the tank was moderately insulated, meaning that this phenomenon is not a major concern on a large scale system with a few hours of standby between charge and discharge. On the 200 MWh injected during charge, around 9 % were provided by the fans, mostly because of the pressure drop in the storage (around 0.11 bar) and the heater (set at 0.15 bar).

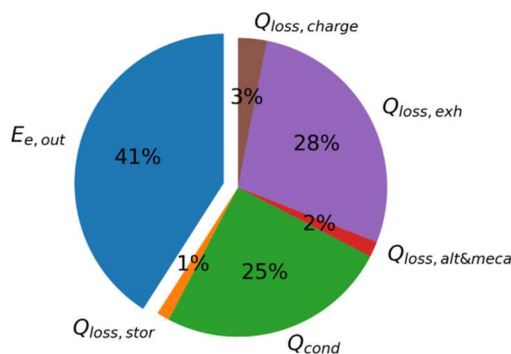


Figure 3. Energy distribution on a whole power-to-power process in the base case.

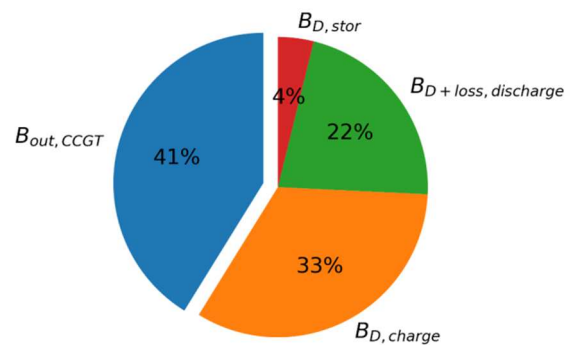


Figure 4. Exergy distribution on the power-to-power process in the base case.

The exergy distribution is shown in Figure 4. In this figure, the exergy lost in the exhaust gases and the mechanical and electric losses have been included in the discharge contribution. From this pie chart, it is clear that most of the exergy destruction happens in the charging phase. The exergy distribution is further detailed in the Grassmann diagram of Figure 5. The exergy flows in and out of the system are drawn in dark orange, and the exergy destructions are drawn in light orange. If 28 % of the energy was lost to the surroundings with the exhaust gases of the HRSG, it only represents a 6 % loss from an exergy point of view. It can be explained by the moderate temperature of these gases (around 198 °C in the present case). It stills represents a loss that could be reduced by a better heat recovery at the HRSG. In Figure 5, the exergy lost in the condenser is combined with the exhaust gases because they both represent an exergy flow lost to the surroundings. The high energy losses at the condenser only represent a minor share of exergy loss (lower

than 1 % of the inlet exergy), because this occurs at a very low temperature with limited recovery potential.

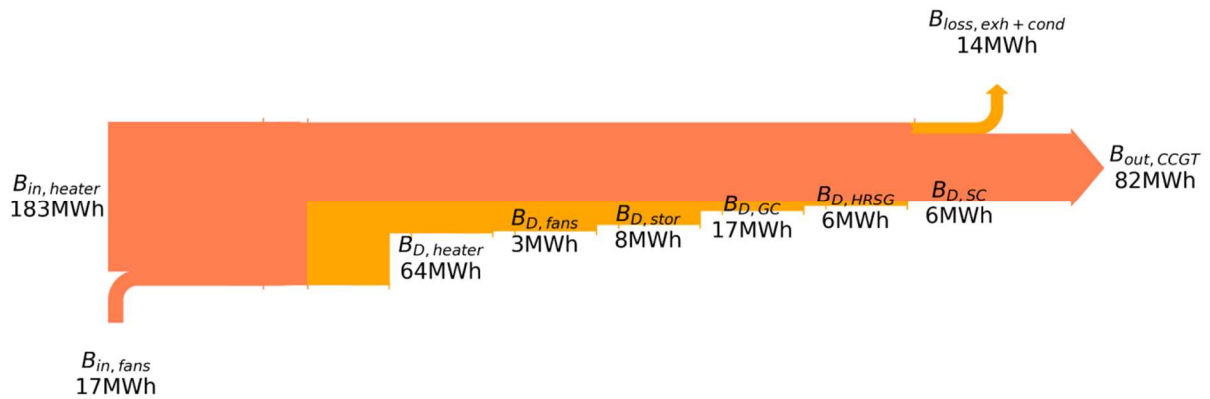


Figure 5. Exergy distribution of the base case in cyclic operation.

The biggest exergy destruction occurs in the electrical heater used to convert electricity into heat. From an exergy point of view, it is an inefficient component by nature, because it converts an energy with an optimal ability to produce work to heat with a moderate conversion potential. These losses could be reduced by increasing the temperature of the heated air. However, this level of temperature was set at 900 °C because of technical constraints. It is still higher than most of the current projects of sensible heat storage with gas as HTF, showing that the temperature probably cannot be further raised. Other exergy destruction sources are the inefficiencies of the turbomachinery, leading to a total of 11 % of exergy destruction in the steam and gas cycles – 14 % if the HRSG is included.

Another result is the share of exergy destruction in the storage compared to the global exergy destruction in the process. This component represents only around 8 % of the global exergy destruction. Several authors showed that this exergy destruction is mainly produced by the convective heat transfer between the fluid and the solids, the pressure drop, the thermal losses and, in a minor extent, to the axial conduction in the fluid and the solids [38]–[40].

5.2. Case 2: release in a combined cycle with combustion at 1200 °C

In this second case, an additional heat input by combustion is used to achieve almost full discharges of the thermal storage, increasing its utilization rate. A moderate combustion temperature of 1200 °C is considered to limit the fuel consumption. As a result of the increase of the GT inlet temperature, the optimal pressure ratio is higher than in the base case. It is found that the optimal thermal efficiency occurs when the pressure ratio is set to 13. The feasibility of a steel vessel for the storage is not the same for a pressure of 10 bar (case 1) and of around 15 bar. The limit dimensions given in Table 2 lead to a maximum of 4.75 m x 4.75 m of useful storage volume in one tank. For this case, the storage volume has to be contained in six tanks operated in parallel. The main thermal model results are shown in Table 6.

Table 6. Thermal model results of the second case (with combustion).

Variable	Value
$V_{stor,tot}$	459 m ³ ($L_b=D_b=4.6\text{m}$, $n_{tanks} = 6$)
\dot{m}_{charge}	75.8 kg.s ⁻¹
$\Delta P_{stor,charge}$	~ 0.04 bar
$\dot{m}_{discharge}$	162 kg.s ⁻¹

PR	13
$P_{in,st}$	72 bar
$E_{e,in}$	200 MWh _e
η_{CCGT}	0.495
$E_{e,out}$	222 MWh _e
$E_{e,out,stor}$	94.8 MWh _e
η_{P2P}	0.475
τ_{stor}	0.96

The results show that the utilization rate of the tanks is close to 100 %. Oversizing is not required anymore (storage volume is 20 % lower than in the base case). Another positive aspect of this architecture is the increase in power-to-power efficiency (+ 8 points when compared to the base case). This can be explained by the higher level of temperature in the combined cycle which leads to a better energy conversion efficiency in this cycle. This power-to-power efficiency could be further increased by setting a higher level of combustion temperature. Meanwhile, it would lead to higher fuel consumption and higher operational costs. If we only consider the heat input from the storage (192 MWh_{th} during the discharge), the output electrical energy with this efficiency is 95 MWh_e, which is 14 % higher than the base case for the same amount of energy. The energy distribution on the power-to-power process is illustrated in Figure 6. It is more or less the same as in the base case. The storage now only represents less than a half of the energy inlet of the combined cycle (the other part being brought by the combustion).

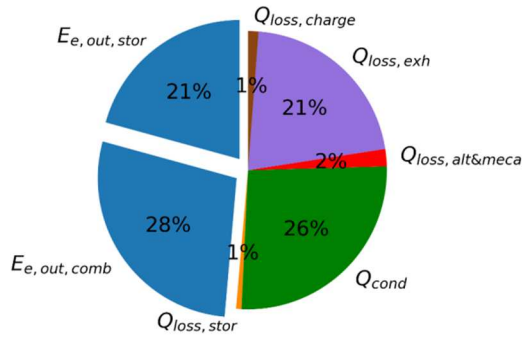


Figure 6. Energy distribution on the power-to-power process in the second case.

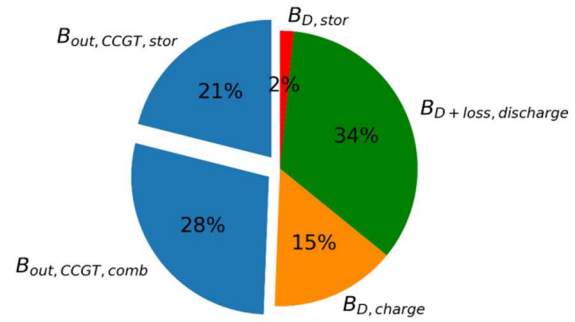


Figure 7. Exergy distribution on the power-to-power process in the second case.

The exergy distribution is shown on the pie chart of Figure 7. For simplification purposes, the inlet exergy from the combustion is assumed to be equal to its LHV value:

$$\dot{B}_{in,comb} = LHV_{CH_4} \dot{m}_{CH_4} \quad (29)$$

The exergy destruction during discharge becomes prevailing. Figure 8 highlights the major increase of exergy destruction in the gas cycle leading to this result. This is mainly due to combustion (63 % of the exergy destroyed in the gas cycle), which is not an exergy efficient process; the incoming fuel having a high exergy value used to produce heat at 1200 °C. Moreover, as can be seen on Figure 8, the electricity injected in the electrical heater and the fans represents merely a half of the exergy inlet of the process, the other half being brought by combustion. The power brought by combustion increases during the discharge, gradually as the temperature at the outlet of the storage decreases. The fuel mass flow rate grows from 1.2 to 2.8 kg.s⁻¹ during the energy release.

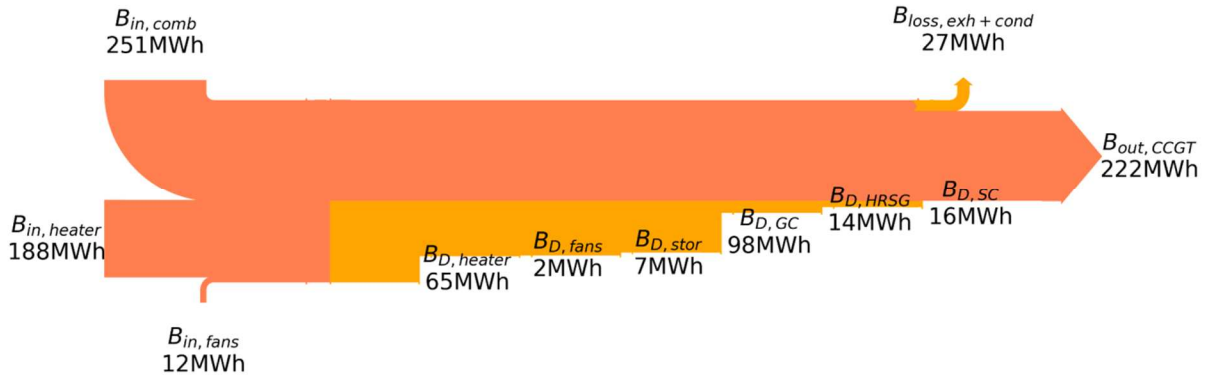


Figure 8. Exergy distribution of the second case in cyclic operation.

The share of exergy destruction in the electrical heater is of the same order of magnitude than in the base case. It remains an important exergy destruction at the whole process scale. It has yet to be compared with the exergy efficiency of more conventional systems with combustion as heat input. In the considered scenario, the electrical heater destroys between 30 and 35 % of its inlet exergy. During discharge, the combustion itself destroys between 22 % (at the beginning of the discharge) to 27 % (at the end) of its inlet exergy. This leads to two interesting conclusions. First of all, the increase in time of the exergy destruction in the combustion process can be explained by the decrease of the temperature at the outlet of the storage. By introducing heat at a high level of temperature in the combustion chamber, the storage therefore brings an interesting benefit to the combustion process during most of the discharging phase. Secondly, in a conventional combustion cycle, the combustion chamber exergy efficiency is limited (around 70 %) [41]. The exergy efficiency of the electrical heater is close to this value. In other words, the inherent exergy inefficiency of the power-to-heat conversion is acceptable when compared to conventional heat inputs by combustion in gas or combined cycles.

5.3. Case 3: release in a gas cycle without combustion

Because a combined cycle involves high investment costs, a decider could desire to know what would be the efficiency of the process with a cheaper discharging subsystem. It will be further investigated by considering a simple gas cycle for the heat to power conversion. In this case, the optimal pressure level of the gas cycle, that is the pressure level which maximizes the thermal efficiency of the cycle, is the maximal pressure that can be reached in the storage tanks: 15 bars. The main thermal model results are shown in Table 7.

Table 7. Thermal model results of the third case (gas cycle).

Variable	Value
$V_{stor,tot}$	688 m ³ ($L_b=D_b=4.6m$, $n_{tanks}=9$)
\dot{m}_{charge}	86.2 kg.s ⁻¹
$\Delta P_{stor,charge}$	~ 0.03 bar
$\dot{m}_{discharge}$	112.5 kg.s ⁻¹
PR	15
$E_{e,in}$	200 MWhe
η_{CCGT}	0.34
$E_{e,out}$	64 MWhe
η_{P2P}	0.32
τ_{stor}	0.66

Without any surprise, the power-to-power efficiency decreases (almost 10 points lower than the base case). This has direct consequences on the outlet energy, which is 23 % lower than in the base case. Energy and exergy distributions are shown in the pie charts of Figures 9 and 10. A lot of energy and exergy is lost in the expanded gases, with a turbine outlet temperature of about 375 °C.

Higher pressure ratio in the gas cycle means a higher compressor outlet temperature, and a lower temperature difference in the storage. This is why the discharge in a gas cycle at its optimal design point also involves a greater storage volume (+ 19 %) than the discharge in a combined cycle (base case). This influence of the pressure ratio can also be found in the combined cycle with combustion (case 2); but the possibility to operate full discharges of the storage lead in this previous case to a decrease of the needed storage volume. Finally, the need for a greater number of tanks due to the higher level of pressure when compared to the base case leads to a lower utilization rate, while the operating conditions stay the same. It can be explained by the increase in thermal losses, as the total external area of the tanks is higher. The higher number of tanks in parallel also leads to a larger total volume filled by the thermal gradient. Both phenomena lead to a utilization rate of 66 %, against 71 % in the base case.

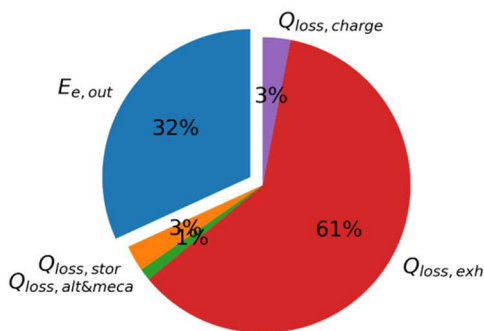


Figure 9. Energy distribution on the power-to-power process in the third case.

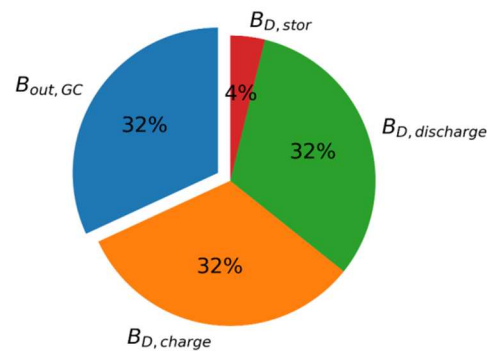


Figure 10. Exergy distribution on the power-to-power process in the third case.

A Grassmann diagram of the exergy distribution is shown in Figure 11. The impact of exergy lost in the exhaust gases appears clearly in this figure, and there is almost the same amount of exergy destroyed in the electrical heater than electricity produced in discharging phase. From an exergy point of view, this cycle is far from efficient.

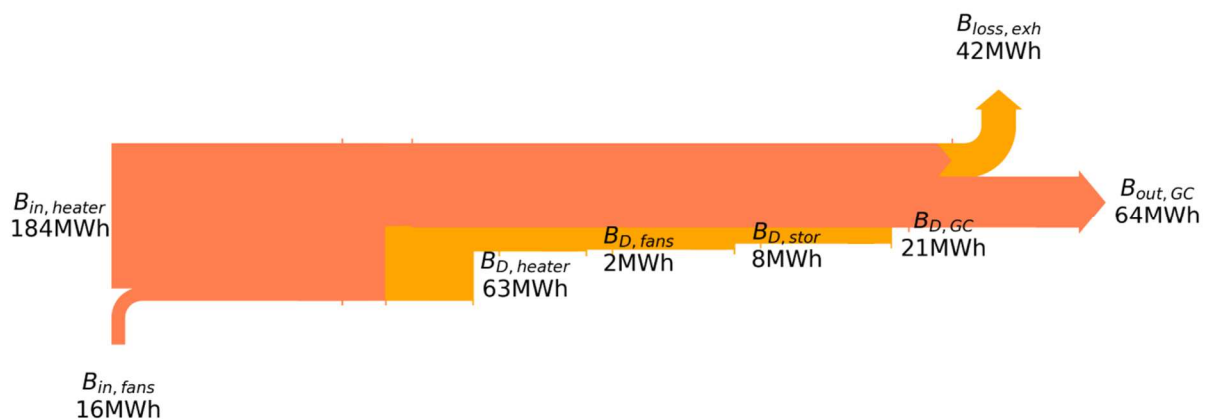


Figure 11. Exergy distribution of the third case in cyclic operation.

5.4. Discussion

The main results of the three case studies are summed up in Table 8.

Table 8. Main results for the three case studies.

Variable	Base case	Case 2	Case 3
<i>Type of cycle</i>	Combined cycle	Combined cycle	Gas cycle
<i>Combustion</i>	No	Yes (251 MWh _{th})	No
$E_{e,in}$	200 MWh _e	200 MWh _e	200 MWh _e
$E_{e,out}$	82 MWh _e	222 MWh _e	64 MWh _e
η_{P2P}	0.41	0.48	0.32
τ_{stor}	0.71	0.96	0.66

A fundamental aspect of this study is that, apart from a few technical aspects, no specific economic considerations were assumed. The considered design constraints were for example the maximal level of temperature of the storage, or the limited dimensions of the tanks due to their level of pressure and temperature. Still, the availability and cost of an electrical heater able to perform a heat-to-electricity conversion at a power of tens of MW and 900 °C has not been verified.

This study introduced an energy and exergy analysis of three 200 MWh electricity storage systems involving sensible thermal energy storage at very high temperature. One of the main conclusions of these analyses is that the thermal storage at high temperature involves limited exergy destructions. Studies could be done to find a way to limit those. For example, McTigue showed that the variation of the specific heat of the solid particles in the considered temperature range has an impact on convective losses because of its influence on the thermal gradient length [38]. Alternative storage materials with different properties could therefore allow to reduce the thermal losses in the storage. Bricks are also often suggested as storage material to avoid high pressure losses when air is used as the heat transfer fluid [42]. Meanwhile, all these improvements would only have limited consequences on the global efficiency of the process, which is more affected by other parameters. Concerning the pressure drop, which is often a concern on great packed bed storage volumes with air as heat transfer fluid, the results showed that a large amount of power is brought by the fans. The designer needs to consider their characteristics to design the storage tanks; the pressure drop for large tanks like those from the base case (around 0.11 bar in charge) being probably a higher limit for usual industrial fans.

This power-to-power concept comes with inherent limited exergy efficiency. The power-to-heat conversion in a Joule heater destroys between 30 and 40 percent of the incoming electrical energy to produce heat at 900 °C. Technical and economical restrictions prevent to reach higher exergy efficiencies by increasing this level of temperature. Meanwhile, it has to be compared with the exergy efficiency of other types of heat inputs for combined cycles. For instance, case 2 showed that the introduction of combustion, even at a moderate level of temperature (1200 °C), led to more exergy destruction in the gas cycle than in the power-to-heat conversion in the Joule heater. On the other hand, designing the system with additional combustion could offer to plug the system in an existing combined cycle or in a project of repowering of an old steam plant. In this case, the system could lead to an interesting hybrid system allowing to reduce the fuel consumption of the plant.

Other typical conclusions of the energy and exergy study of combined cycles apply here. In a gas cycle, exhaust gases represent a high share of energy and exergy loss (around 60 % of the inlet energy in case 3, which only has an incoming heat supply at 900 °C). Recovery of this heat loss with a steam cycle is the usual proposal of the combined cycles to improve the

efficiency of the process. The exhaust gases loss still represents between 21 % and 27 % of the incoming energy of the combined cycle in cases 1 and 2. A better heat recovery in the HRSG could be a way to reduce these losses. Adding a level of vaporization pressure is a common solution [43].

With the results of this study, the proposed system can be compared with other storage technologies. In terms of massive electricity storage technologies, its main competitors could be PHS, CAES, batteries or systems with lower technological maturity like pumped thermal electricity storage. The best round-trip efficiency is found for the case with combustion (case 2) at around 50 %. PHS can lead to round trip efficiencies of 70-80 % [2]. CAES stands around 40-50 % for the existing plants (Huntorf and McIntosh). Studies on A-CAES show that adding a thermal storage could lead to an efficiency of about 70 % [7]. The round-trip efficiency of the proposed system is therefore similar to the efficiency of conventional CAES systems. It remains lower than the efficiency of the PHS or the A-CAES processes, but the proposed system has a main advantage on these systems, being its ability to be plugged anywhere. Furthermore, the scalability of batteries to store high amounts of energy can be difficult. Finally, innovative systems like pumped thermal electricity storage could offer theoretical round-trip efficiencies of about 85 % [4], but the proposed system relies on more mature components and its short term feasibility seems easier.

This thermodynamic study could be used to carry out an economic evaluation of the three cases. Such an analysis is available in reference [44], which shows that the levelized cost of energy storage is slightly higher than the one of PHS or CAES, but it is competitive with batteries, for instance. It also shows that despite its inefficiencies, the energy release in a gas cycle leads to higher profitability because of the great influence of lower investment costs at the concerned levels of power and energy (see ref [44] and [45] for more details).

6. Conclusion

This study showed that a power-to-power storage system involving the hybridization of high temperature thermal energy storage with a combined cycle could lead to round-trip-efficiencies between 40 % and 50 %. Combustion improves the discharging cycle efficiency and gives a better valorization of the stored energy. Moreover, by increasing the utilization rate of the storage tanks, the combustion reduces by about 20 % the volume of the storage to store the same amount of energy. The addition of the charging process comes with inherent exergy losses due to the electricity to heat conversion, even if this conversion has a good energy efficiency.

Simulations were also carried out to evaluate the efficiency of the discharge in a simple gas cycle without additional combustion. For a same amount of stored energy, the output power is reduced by more than 20 %. Moreover, to get an optimal efficiency with such a cycle, the pressure level of the gas cycle needs to be higher than the optimal pressure level of a combined cycle. It means that the storage tanks are exposed to higher pressure, which can affect their feasibility and sizing.

With the results of this study, several design aspects from the power-to-power system with thermal storage have been covered. The results clearly show that the next step should be an optimization of the system, based on exergy and cost indicators. The remaining design uncertainties are indeed linked to economical and cost considerations. For example, the decrease of storage volumes brought by combustion needs to be put in perspective with the additional cost of the fuel. In a similar way, only a cost analysis would tell if a simple gas cycle should be considered for the discharging process, even if its poor performances from a thermodynamic point of view have been highlighted.

Acknowledgements

This work was supported by BPIFrance, the Nouvelle-Aquitaine and Babcock Wanson, as part of the EMR'Stock project from the FUI 17 program.

References

- [1] REN21. 2017., *Renewables 2017 Global Status Report*. Paris: REN21 Secretariat.
- [2] H. Chen, T. N. Cong, W. Yang, C. Tan, Y. Li, and Y. Ding, "Progress in electrical energy storage system: A critical review," *Prog. Nat. Sci.*, vol. 19, no. 3, pp. 291–312, Mar. 2009.
- [3] T. Desrues, J. Ruer, P. Marty, and J. F. Fourmigué, "A thermal energy storage process for large scale electric applications," *Appl. Therm. Eng.*, vol. 30, no. 5, pp. 425–432, Apr. 2010.
- [4] J. D. McTigue, A. J. White, and C. N. Markides, "Parametric studies and optimisation of pumped thermal electricity storage," *Appl. Energy*, vol. 137, pp. 800–811, Jan. 2015.
- [5] I. Ortega-Fernández, S. A. Zavattoni, J. Rodríguez-Aseguinolaza, B. D'Aguanno, and M. C. Barbato, "Analysis of an integrated packed bed thermal energy storage system for heat recovery in compressed air energy storage technology," *Appl. Energy*, vol. 205, pp. 280–293, Nov. 2017.
- [6] A. Benato, "Performance and cost evaluation of an innovative Pumped Thermal Electricity Storage power system," *Energy*, vol. 138, pp. 419–436, Nov. 2017.
- [7] A. Kéré, V. Goetz, X. Py, R. Olives, and N. Sadiki, "Modeling and integration of a heat storage tank in a compressed air electricity storage process," *Energy Convers. Manag.*, vol. 103, pp. 499–510, Oct. 2015.
- [8] A. Gil *et al.*, "State of the art on high temperature thermal energy storage for power generation. Part 1—Concepts, materials and modellization," *Renew. Sustain. Energy Rev.*, vol. 14, no. 1, pp. 31–55, Jan. 2010.
- [9] T. Esence, A. Bruch, S. Molina, B. Stutz, and J.-F. Fourmigué, "A review on experience feedback and numerical modeling of packed-bed thermal energy storage systems," *Sol. Energy*, vol. 153, pp. 628–654, Sep. 2017.
- [10] M. Medrano, A. Gil, I. Martorell, X. Potau, and L. F. Cabeza, "State of the art on high-temperature thermal energy storage for power generation. Part 2—Case studies," *Renew. Sustain. Energy Rev.*, vol. 14, no. 1, pp. 56–72, Jan. 2010.
- [11] T. Fasquelle, Q. Falcoz, P. Neveu, and J.-F. Hoffmann, "A temperature threshold evaluation for thermocline energy storage in concentrated solar power plants," *Appl. Energy*, vol. 212, pp. 1153–1164, Feb. 2018.
- [12] M. Y. Haller, C. A. Cruickshank, W. Streicher, S. J. Harrison, E. Andersen, and S. Furbo, "Methods to determine stratification efficiency of thermal energy storage processes – Review and theoretical comparison," *Sol. Energy*, vol. 83, no. 10, pp. 1847–1860, Oct. 2009.
- [13] D. Okello, O. J. Nydal, and E. J. K. Banda, "Experimental investigation of thermal de-stratification in rock bed TES systems for high temperature applications," *Energy Convers. Manag.*, vol. 86, pp. 125–131, Oct. 2014.
- [14] H. Agalit, N. Zari, M. Maalmi, and M. Maaroufi, "Numerical investigations of high temperature packed bed TES systems used in hybrid solar tower power plants," *Sol. Energy*, vol. 122, pp. 603–616, Dec. 2015.
- [15] R. Anderson, S. Shiri, H. Bindra, and J. F. Morris, "Experimental results and modeling of energy storage and recovery in a packed bed of alumina particles," *Appl. Energy*, vol. 119, pp. 521–529, Apr. 2014.

- [16]G. Zanganeh, A. Pedretti, A. Haselbacher, and A. Steinfeld, "Design of packed bed thermal energy storage systems for high-temperature industrial process heat," *Appl. Energy*, vol. 137, pp. 812–822, Jan. 2015.
- [17]G. Zanganeh, A. Pedretti, S. A. Zavattoni, M. C. Barbato, A. Haselbacher, and A. Steinfeld, "Design of a 100 MWhth Packed-bed Thermal Energy Storage," *Energy Procedia*, vol. 49, pp. 1071–1077, 2014.
- [18]K.-Y. Wang, R. E. West, F. Kreith, and P. Lynn, "High-temperature sensible-heat storage options," *Energy*, vol. 10, no. 10, pp. 1165–1175, 1985.
- [19]VentMeca Fans SAS, "Ventilateurs industriels - Brochure.", http://www.ventmeca.fr/medias/documents_textes/documents_et_outils/ventmeca_fans.pdf [accessed on 22 October 2018]
- [20]M. A. Korobitsyn, "New and advanced energy conversion technologies: analysis of cogeneration, combined and integrated cycles," University of Twente, Enschede, 1998.
- [21]R. Daschner, S. Binder, and M. Mocker, "Pebble bed regenerator and storage system for high temperature use," *Appl. Energy*, vol. 109, pp. 394–401, 2013.
- [22]R. G. Munro, "Evaluated Material Properties for a Sintered alpha-Alumina," *J. Am. Ceram. Soc.*, vol. 80, no. 8, pp. 1919–1928, 1997.
- [23]L. Mongibello, M. Atrigna, and G. Graditi, "Parametric analysis of a high temperature sensible heat storage system by numerical simulations," *J. Sol. Energy Eng.*, vol. 135, no. 4, p. 041010, 2013.
- [24]J. D. Spelling, "Hybrid solar gas-turbine power plants: a thermoeconomic analysis," KTH Royal Institute of Technology, Stockholm, 2013.
- [25]A. L. Polyzakis, C. Koroneos, and G. Xydis, "Optimum gas turbine cycle for combined cycle power plant," *Energy Convers. Manag.*, vol. 49, no. 4, pp. 551–563, Apr. 2008.
- [26]A. Rovira, C. Sánchez, and M. Muñoz, "Analysis and optimisation of combined cycles gas turbines working with partial recuperation," *Energy Convers. Manag.*, vol. 106, pp. 1097–1108, Dec. 2015.
- [27]Spirax Sarco, "Pressurised Deaerators," *Steam Engineering Tutorials - The Boiler House*, <http://www.spiraxsarco.com/Resources/Pages/Steam-Engineering-Tutorials/the-boiler-house/pressurised-deaerators.aspx> [accessed on 22 October 2018]
- [28]D. E. Beasley and J. A. Clark, "Transient response of a packed bed for thermal energy storage," *Int. J. Heat Mass Transf.*, vol. 27, no. 9, pp. 1659–1669, Sep. 1984.
- [29]K. A. R. Ismail and R. Stuginsky Jr, "A parametric study on possible fixed bed models for pcm and sensible heat storage," *Appl. Therm. Eng.*, vol. 19, no. 7, pp. 757–788, Jul. 1999.
- [30]B. Stuke, "Berechnung des Wärmeaustausches in Regeneratoren mit zylindrischen und kugelförmigen Füllmaterial," *Angew. Chem.*, vol. B20, p. 262, 1948.
- [31]B. Xu, P.-W. Li, and C. L. Chan, "Extending the validity of lumped capacitance method for large Biot number in thermal storage application," *Sol. Energy*, vol. 86, no. 6, pp. 1709–1724, Jun. 2012.
- [32]N. Wakao, S. Kaguei, and T. Funazkri, "Effect of fluid dispersion coefficients on particle-to-fluid heat transfer coefficients in packed beds," *Chem. Eng. Sci.*, vol. 34, no. 3, pp. 325–336, 1979.
- [33]P. Zehner and E. U. Schlünder, "Wärmeleitfähigkeit von Schüttungen bei mäßigen Temperaturen," *Chem. Ing. Tech.*, vol. 42, no. 14, pp. 933–941, Jul. 1970.

- [34]G. Breitbach and H. Barthels, "The radiant heat transfer in the high temperature reactor core after failure of the afterheat removal systems," *Nucl. Technol.*, vol. 49, no. 3, pp. 392–399, 1980.
- [35]N. Wakao and S. Kagei, *Heat and Mass Transfer in Packed Beds*. Taylor & Francis, 1982.
- [36]S. Ergun, "Fluid flow through packed columns," *Chem. Eng. Prog.*, vol. 48, no. 2, pp. 89–94, 1952.
- [37]A. Bejan, G. Tsatsaronis, and M. Moran, *Thermal Design and Optimization*. John Wiley & Sons, Inc., 1995.
- [38]J. D. McTigue, "Analysis and optimisation of thermal energy storage," Cambridge, St. Catherine's College, 2016.
- [39]A. De Waele, P. P. Steijaert, and J. Gijzen, "Thermodynamical aspects of pulse tubes," *Cryogenics*, vol. 37, no. 6, pp. 313–324, 1997.
- [40]A. Bejan, "Two Thermodynamic Optima in the Design of Sensible Heat Units for Energy Storage," *J. Heat Transf.*, vol. 100, no. 4, pp. 708–712, Nov. 1978.
- [41]H. Taniguchi, K. Mouri, T. Nakahara, and N. Arai, "Exergy analysis on combustion and energy conversion processes," *Energy*, vol. 30, no. 2–4, pp. 111–117, Feb. 2005.
- [42]S. Kuravi, J. Trahan, Y. Goswami, C. Jotshi, E. Stefanakos, and N. Goel, "Investigation of a high-temperature packed-bed sensible heat thermal energy storage system with large-sized elements," *J. Sol. Energy Eng.*, vol. 135, no. 4, p. 041008, 2013.
- [43]A. Rovira, C. Sánchez, M. Muñoz, M. Valdés, and M. D. Durán, "Thermoeconomic optimisation of heat recovery steam generators of combined cycle gas turbine power plants considering off-design operation," *Energy Convers. Manag.*, vol. 52, no. 4, pp. 1840–1849, Apr. 2011.
- [44]K. Attonaty, J. Pouvreau, A. Deydier, J. Oriol, and P. Stouffs, "Thermodynamic and economic evaluation of an innovative electricity storage system based on thermal energy storage," in *Proceedings of ECOS 2018*, Guimaraes, Portugal, 2018.
- [45]K. Attonaty, "Stockage d'électricité associant un cycle thermodynamique à haut rendement avec un stockage thermique à haute température," PhD Thesis, Université de Pau et des Pays de l'Adour, 2018.